

Search for New Particles Decaying to $b\bar{b}$ in $p\bar{p}$ Collisions at $\sqrt{s} = 1.8$ TeV

- F. Abe,¹⁷ H. Akimoto,³⁹ A. Akopian,³¹ M. G. Albrow,⁷ A. Amadon,⁵ S. R. Amendolia,²⁷ D. Amidei,²⁰ J. Antos,³³ S. Aota,³⁷ G. Apollinari,³¹ T. Arisawa,³⁹ T. Asakawa,³⁷ W. Ashmanskas,¹⁸ M. Atac,⁷ P. Azzi-Bacchetta,²⁵ N. Bacchetta,²⁵ S. Bagdasarov,³¹ M. W. Bailey,²² J. Bao,⁴¹ P. de Barbaro,³⁰ A. Barbaro-Galtieri,¹⁸ V. E. Barnes,²⁹ B. A. Barnett,¹⁵ M. Barone,⁹ G. Bauer,¹⁹ T. Baumann,¹¹ F. Bedeschi,²⁷ S. Behrends,³ S. Belforte,²⁷ G. Bellettini,²⁷ J. Bellinger,⁴⁰ D. Benjamin,³⁵ J. Bensinger,³ A. Beretvas,⁷ J. P. Berge,⁷ J. Berryhill,⁵ S. Bertolucci,⁹ S. Bettelli,²⁷ B. Bevensee,²⁶ A. Bhatti,³¹ K. Biery,⁷ C. Bigongiari,²⁷ M. Binkley,⁷ D. Bisello,²⁵ R. E. Blair,¹ C. Blocker,³ K. Bloom,²⁰ S. Blusk,³⁰ A. Bodek,³⁰ W. Bokhari,²⁶ G. Bolla,²⁹ Y. Bonushkin,⁴ D. Bortoletto,²⁹ J. Boudreau,²⁸ L. Breccia,² C. Bromberg,²¹ N. Bruner,²² R. Brunetti,² E. Buckley-Geer,⁷ H. S. Budd,³⁰ K. Burkett,¹¹ G. Busetto,²⁵ A. Byon-Wagner,⁷ K. L. Byrum,¹ M. Campbell,²⁰ A. Caner,²⁷ W. Carithers,¹⁸ D. Carlsmith,⁴⁰ J. Cassada,³⁰ A. Castro,²⁵ D. Cauz,³⁶ A. Cerri,²⁷ P. S. Chang,³³ P. T. Chang,³³ H. Y. Chao,³³ J. Chapman,²⁰ M. -T. Cheng,³³ M. Chertok,³⁴ G. Chiarelli,²⁷ C. N. Chiou,³³ F. Chlebana,⁷ L. Christofek,¹³ R. Cropp,¹⁴ M. L. Chu,³³ S. Cihangir,⁷ A. G. Clark,¹⁰ M. Cobal,²⁷ E. Cocca,²⁷ M. Contreras,⁵ J. Conway,³² J. Cooper,⁷ M. Cordelli,⁹ D. Costanzo,²⁷ C. Couyoumtzelis,¹⁰ D. Cronin-Hennessy,⁶ R. Culbertson,⁵ D. Dagenhart,³⁸ T. Daniels,¹⁹ F. DeJongh,⁷ S. Dell'Agnello,⁹ M. Dell'Orso,²⁷ R. Demina,⁷ L. Demortier,³¹ M. Deninno,² P. F. Derwent,⁷ T. Devlin,³² J. R. Dittmann,⁶ S. Donati,²⁷ J. Done,³⁴ T. Dorigo,²⁵ N. Eddy,¹³ K. Einsweiler,¹⁸ J. E. Elias,⁷ R. Ely,¹⁸ E. Engels, Jr.,²⁸ W. Erdmann,⁷ D. Errede,¹³ S. Errede,¹³ Q. Fan,³⁰ R. G. Feild,⁴¹ Z. Feng,¹⁵ C. Ferretti,²⁷ I. Fiori,² B. Flaucher,⁷ G. W. Foster,⁷ M. Franklin,¹¹ J. Freeman,⁷ J. Friedman,¹⁹ H. Frisch,⁵ Y. Fukui,¹⁷ S. Gadomski,¹⁴ S. Galeotti,²⁷ M. Gallinaro,²⁶ O. Ganel,³⁵ M. Garcia-Sciveres,¹⁸ A. F. Garfinkel,²⁹ C. Gay,⁴¹ S. Geer,⁷ D. W. Gerdes,²⁰ P. Giannetti,²⁷ N. Giokaris,³¹ P. Giromini,⁹ G. Giusti,²⁷ M. Gold,²² A. Gordon,¹¹ A. T. Goshaw,⁶ Y. Gotra,²⁸ K. Goulianatos,³¹ H. Grassmann,³⁶ L. Groer,³² C. Grossos-Pilcher,⁵ G. Guillian,²⁰ J. Guimaraes da Costa,¹⁵ R. S. Guo,³³ C. Haber,¹⁸ E. Hafen,¹⁹ S. R. Hahn,⁷ R. Hamilton,¹¹ T. Handa,¹² R. Handler,⁴⁰ W. Hao,³⁵ F. Happacher,⁹ K. Hara,³⁷ A. D. Hardman,²⁹ R. M. Harris,⁷ F. Hartmann,¹⁶ J. Hauser,⁴ E. Hayashi,³⁷ J. Heinrich,²⁶ A. Heiss,¹⁶ B. Hinrichsen,¹⁴ K. D. Hoffman,²⁹ M. Hohlmann,⁵ C. Holck,²⁶ R. Hollebeek,²⁶ L. Holloway,¹³ Z. Huang,²⁰ B. T. Huffman,²⁸ R. Hughes,²³ J. Huston,²¹ J. Huth,¹¹ H. Ikeda,³⁷ M. Incagli,²⁷ J. Incandela,⁷ G. Introzzi,²⁷ J. Iwai,³⁹ Y. Iwata,¹² E. James,²⁰ H. Jensen,⁷ U. Joshi,⁷ E. Kajfasz,²⁵ H. Kambara,¹⁰ T. Kamon,³⁴ T. Kaneko,³⁷ K. Karr,³⁸ H. Kasha,⁴¹ Y. Kato,²⁴ T. A. Keaffaber,²⁹ K. Kelley,¹⁹ R. D. Kennedy,⁷ R. Kephart,⁷ D. Kestenbaum,¹¹ D. Khazins,⁶ T. Kikuchi,³⁷ B. J. Kim,²⁷ H. S. Kim,¹⁴ S. H. Kim,³⁷ Y. K. Kim,¹⁸ L. Kirsch,³ S. Klimentko,⁸ D. Knoblauch,¹⁶ P. Koehn,²³ A. Köngeter,¹⁶ K. Kondo,³⁷ J. Konigsberg,⁸ K. Kordas,¹⁴ A. Korytov,⁸ E. Kovacs,¹

W. Kowald,⁶ J. Kroll,²⁶ M. Kruse,³⁰ S. E. Kuhlmann,¹ E. Kuns,³² K. Kurino,¹²
 T. Kuwabara,³⁷ A. T. Laasanen,²⁹ S. Lami,²⁷ S. Lammel,⁷ J. I. Lamoureux,³
 M. Lancaster,¹⁸ M. Lanzoni,²⁷ G. Latino,²⁷ T. LeCompte,¹ S. Leone,²⁷ J. D. Lewis,⁷
 M. Lindgren,⁴ T. M. Liss,¹³ J. B. Liu,³⁰ Y. C. Liu,³³ N. Lockyer,²⁶ O. Long,²⁶
 M. Loretti,²⁵ D. Lucchesi,²⁷ P. Lukens,⁷ S. Lusin,⁴⁰ J. Lys,¹⁸ K. Maeshima,⁷
 P. Maksimovic,¹¹ M. Mangano,²⁷ M. Mariotti,²⁵ J. P. Marriner,⁷ G. Martignon,²⁵
 A. Martin,⁴¹ J. A. J. Matthews,²² P. Mazzanti,² K. McFarland,³⁰ P. McIntyre,³⁴
 P. Melese,³¹ M. Menguzzato,²⁵ A. Menzione,²⁷ E. Meschi,²⁷ S. Metzler,²⁶ C. Miao,²⁰
 T. Miao,⁷ G. Michail,¹¹ R. Miller,²¹ H. Minato,³⁷ S. Miscetti,⁹ M. Mishina,¹⁷
 S. Miyashita,³⁷ N. Moggi,²⁷ E. Moore,²² Y. Morita,¹⁷ A. Mukherjee,⁷ T. Muller,¹⁶
 P. Murat,²⁷ S. Murgia,²¹ M. Musy,³⁶ H. Nakada,³⁷ T. Nakaya,⁵ I. Nakano,¹²
 C. Nelson,⁷ D. Neuberger,¹⁶ C. Newman-Holmes,⁷ C.-Y. P. Ngan,¹⁹ L. Nodulman,¹
 A. Nomerotski,⁸ S. H. Oh,⁶ T. Ohmoto,¹² T. Ohsugi,¹² R. Oishi,³⁷ M. Okabe,³⁷
 T. Okusawa,²⁴ J. Olsen,⁴⁰ C. Pagliarone,²⁷ R. Paoletti,²⁷ V. Papadimitriou,³⁵
 S. P. Pappas,⁴¹ N. Parashar,²⁷ A. Parri,⁹ J. Patrick,⁷ G. Pauletta,³⁶ M. Paulini,¹⁸
 A. Perazzo,²⁷ L. Pescara,²⁵ M. D. Peters,¹⁸ T. J. Phillips,⁶ G. Piacentino,²⁷ M. Pillai,³⁰
 K. T. Pitts,⁷ R. Plunkett,⁷ A. Pompos,²⁹ L. Pondrom,⁴⁰ J. Proudfoot,¹ F. Ptohos,¹¹
 G. Punzi,²⁷ K. Ragan,¹⁴ D. Reher,¹⁸ M. Reischl,¹⁶ A. Ribon,²⁵ F. Rimondi,²
 L. Ristori,²⁷ W. J. Robertson,⁶ A. Robinson,¹⁴ T. Rodrigo,²⁷ S. Rolli,³⁸ L. Rosenson,¹⁹
 R. Roser,¹³ T. Saab,¹⁴ W. K. Sakumoto,³⁰ D. Saltzberg,⁴ A. Sansoni,⁹ L. Santi,³⁶
 H. Sato,³⁷ P. Schlabach,⁷ E. E. Schmidt,⁷ M. P. Schmidt,⁴¹ A. Scott,⁴ A. Scribano,²⁷
 S. Segler,⁷ S. Seidel,²² Y. Seiya,³⁷ F. Semeria,² T. Shah,¹⁹ M. D. Shapiro,¹⁸
 N. M. Shaw,²⁹ P. F. Shepard,²⁸ T. Shibayama,³⁷ M. Shimojima,³⁷ M. Shochet,⁵
 J. Siegrist,¹⁸ A. Sill,³⁵ P. Sinervo,¹⁴ P. Singh,¹³ K. Sliwa,³⁸ C. Smith,¹⁵ F. D. Snider,¹⁵
 J. Spalding,⁷ T. Speer,¹⁰ P. Sphicas,¹⁹ F. Spinella,²⁷ M. Spiropulu,¹¹ L. Spiegel,⁷
 L. Stanco,²⁵ J. Steele,⁴⁰ A. Stefanini,²⁷ R. Ströhmer,^{7a} J. Strologas,¹³ F. Strumia,¹⁰
 D. Stuart,⁷ K. Sumorok,¹⁹ J. Suzuki,³⁷ T. Suzuki,³⁷ T. Takahashi,²⁴ T. Takano,²⁴
 R. Takashima,¹² K. Takikawa,³⁷ M. Tanaka,³⁷ B. Tannenbaum,⁴ F. Tartarelli,²⁷
 W. Taylor,¹⁴ M. Tecchio,²⁰ P. K. Teng,³³ Y. Teramoto,²⁴ K. Terashi,³⁷ S. Tether,¹⁹
 D. Theriot,⁷ T. L. Thomas,²² R. Thurman-Keup,¹ M. Timko,³⁸ P. Tipton,³⁰
 A. Titov,³¹ S. Tkaczyk,⁷ D. Toback,⁵ K. Tollefson,³⁰ A. Tollestrup,⁷ H. Toyoda,²⁴
 W. Trischuk,¹⁴ J. F. de Troconiz,¹¹ S. Truitt,²⁰ J. Tseng,¹⁹ N. Turini,²⁷ T. Uchida,³⁷
 F. Ukegawa,²⁶ J. Valls,³² S. C. van den Brink,¹⁵ S. Vejcik, III,²⁰ G. Velev,²⁷
 R. Vidal,⁷ R. Vilar,^{7a} D. Vucinic,¹⁹ R. G. Wagner,¹ R. L. Wagner,⁷ J. Wahl,⁵
 N. B. Wallace,²⁷ A. M. Walsh,³² C. Wang,⁶ C. H. Wang,³³ M. J. Wang,³³
 A. Warburton,¹⁴ T. Watanabe,³⁷ T. Watts,³² R. Webb,³⁴ C. Wei,⁶ H. Wenzel,¹⁶
 W. C. Wester, III,⁷ A. B. Wicklund,¹ E. Wicklund,⁷ R. Wilkinson,²⁶ H. H. Williams,²⁶
 P. Wilson,⁷ B. L. Winer,²³ D. Winn,²⁰ D. Wolinski,²⁰ J. Wolinski,²¹ S. Worm,²²
 X. Wu,¹⁰ J. Wyss,²⁷ A. Yagil,⁷ W. Yao,¹⁸ K. Yasuoka,³⁷ G. P. Yeh,⁷ P. Yeh,³³ J. Yoh,⁷
 C. Yosef,²¹ T. Yoshida,²⁴ I. Yu,⁷ A. Zanetti,³⁶ F. Zetti,²⁷ and S. Zucchelli²

(CDF Collaboration)

- ¹ Argonne National Laboratory, Argonne, Illinois 60439
² Istituto Nazionale di Fisica Nucleare, University of Bologna, I-40127 Bologna, Italy
³ Brandeis University, Waltham, Massachusetts 02254
⁴ University of California at Los Angeles, Los Angeles, California 90024
⁵ University of Chicago, Chicago, Illinois 60637
⁶ Duke University, Durham, North Carolina 27708
⁷ Fermi National Accelerator Laboratory, Batavia, Illinois 60510
⁸ University of Florida, Gainesville, Florida 32611
⁹ Laboratori Nazionali di Frascati, Istituto Nazionale di Fisica Nucleare, I-00044 Frascati, Italy
¹⁰ University of Geneva, CH-1211 Geneva 4, Switzerland
¹¹ Harvard University, Cambridge, Massachusetts 02138
¹² Hiroshima University, Higashi-Hiroshima 724, Japan
¹³ University of Illinois, Urbana, Illinois 61801
¹⁴ Institute of Particle Physics, McGill University, Montreal H3A 2T8, and University of Toronto, Toronto M5S 1A7, Canada
¹⁵ The Johns Hopkins University, Baltimore, Maryland 21218
¹⁶ Institut für Experimentelle Kernphysik, Universität Karlsruhe, 76128 Karlsruhe, Germany
¹⁷ National Laboratory for High Energy Physics (KEK), Tsukuba, Ibaraki 305, Japan
¹⁸ Ernest Orlando Lawrence Berkeley National Laboratory, Berkeley, California 94720
¹⁹ Massachusetts Institute of Technology, Cambridge, Massachusetts 02139
²⁰ University of Michigan, Ann Arbor, Michigan 48109
²¹ Michigan State University, East Lansing, Michigan 48824
²² University of New Mexico, Albuquerque, New Mexico 87131
²³ The Ohio State University, Columbus, Ohio 43210
²⁴ Osaka City University, Osaka 588, Japan
²⁵ Universita di Padova, Istituto Nazionale di Fisica Nucleare, Sezione di Padova, I-35131 Padova, Italy
²⁶ University of Pennsylvania, Philadelphia, Pennsylvania 19104
²⁷ Istituto Nazionale di Fisica Nucleare, University and Scuola Normale Superiore of Pisa, I-56100 Pisa, Italy
²⁸ University of Pittsburgh, Pittsburgh, Pennsylvania 15260
²⁹ Purdue University, West Lafayette, Indiana 47907
³⁰ University of Rochester, Rochester, New York 14627
³¹ Rockefeller University, New York, New York 10021
³² Rutgers University, Piscataway, New Jersey 08855
³³ Academia Sinica, Taipei, Taiwan 11530, Republic of China
³⁴ Texas A&M University, College Station, Texas 77843
³⁵ Texas Tech University, Lubbock, Texas 79409
³⁶ Istituto Nazionale di Fisica Nucleare, University of Trieste/ Udine, Italy
³⁷ University of Tsukuba, Tsukuba, Ibaraki 315, Japan
³⁸ Tufts University, Medford, Massachusetts 02155
³⁹ Waseda University, Tokyo 169, Japan
⁴⁰ University of Wisconsin, Madison, Wisconsin 53706
⁴¹ Yale University, New Haven, Connecticut 06520

Abstract

We have used 87 pb^{-1} of data collected with the Collider Detector at Fermilab to search for new particles decaying to $b\bar{b}$. We present model-independent upper limits on the cross section for narrow resonances which exclude the color-octet technirho in the mass interval $350 < M < 440 \text{ GeV}/c^2$. In addition, we exclude topgluons, predicted in models of topcolor-assisted technicolor, of width $\Gamma = 0.3M$ in the mass range $280 < M < 670 \text{ GeV}/c^2$, of width $\Gamma = 0.5M$ in the mass range $340 < M < 640 \text{ GeV}/c^2$, and of width $\Gamma = 0.7M$ in the mass range $375 < M < 560 \text{ GeV}/c^2$.

PACS numbers: 13.85.Rm, 12.38.Qk, 14.70.Pw, 14.80.-j

In this paper we report on a search for new particles decaying to $b\bar{b}$. In addition to a model independent search for narrow resonances, we perform a specific search for resonances from topcolor-assisted technicolor [1]. Since electroweak symmetry breaking is associated with the origin of fermion masses, the large mass of the top quark suggests that the third generation could contain clues about the origin of electroweak symmetry breaking. Topcolor-assisted technicolor is a model in which the top quark is heavy because of a new interaction. Topcolor replaces the $SU(3)_C$ of QCD with $SU(3)_1$ which couples only to the first two quark generations and $SU(3)_2$ which couples only to the third generation. The symmetry $SU(3)_1 \times SU(3)_2$ is broken, resulting in the familiar $SU(3)_C$ of QCD and an additional $SU(3)$ which couples mainly to the third generation. In addition, there is a $U(1)$ symmetry added to keep the b quark light. The additional $SU(3)$ symmetry gives rise to a color-octet gauge boson, the topgluon g_T , while the additional $U(1)$ symmetry gives rise to a new heavy neutral gauge boson, the topcolor Z'_T . Topgluons are expected to have a large width, so we search for three different widths $\Gamma = 0.3M$, $0.5M$, and $0.7M$, where M is the new particle's mass. For narrow resonances we consider color-octet technirhos from a model of walking technicolor [2], a Z' from topcolor-assisted technicolor [1], a Z' with standard model couplings [3], and a vector bound state of gluinos (vector gluonium) appearing in supersymmetry models [4]. We search for these new phenomena in the $b\bar{b}$ mass spectrum in $p\bar{p}$ collisions at a center of mass energy $\sqrt{s} = 1.8$ TeV.

A detailed description of the Collider Detector at Fermilab (CDF) can be found elsewhere [5]. We use a coordinate system with the z axis along the proton beam,

transverse coordinate perpendicular to the beam, azimuthal angle ϕ , polar angle θ , and pseudorapidity $\eta = -\ln \tan(\theta/2)$. The silicon vertex detector (SVX), a four-layer silicon strip device with radiation-hard electronics, located immediately outside the beampipe, provides precise track reconstruction in the transverse plane and is used to identify secondary-vertices from b quark decays. The momenta of charged particles are measured in the Central Tracking Chamber (CTC), which is inside a 1.4 T superconducting solenoidal magnet. Outside the CTC, electromagnetic and hadronic calorimeters, segmented in η - ϕ towers, cover the pseudorapidity region $|\eta| < 4.2$.

Jets are reconstructed as localized energy depositions in the CDF calorimeters. The jet energy E is defined as the scalar sum of the calorimeter tower energies inside a cone of radius $R = \sqrt{(\Delta\eta)^2 + (\Delta\phi)^2} = 0.7$, centered on the jet direction. The jet momentum \vec{P} is the corresponding vector sum: $\vec{P} = \sum E_i \hat{u}_i$ with \hat{u}_i being the unit vector pointing from the interaction point to the energy deposition E_i in tower i inside the same cone. E and \vec{P} are corrected for calorimeter non-linearities, energy lost in uninstrumented regions of the detector and outside the clustering cone, and energy gained from the underlying event and multiple $p\bar{p}$ interactions. Full details of jet reconstruction and jet energy corrections at CDF can be found elsewhere [6].

We define the dijet system as the two jets with the highest transverse momentum in an event (leading jets) and define the dijet mass $m = \sqrt{(E_1 + E_2)^2 - (\vec{P}_1 + \vec{P}_2)^2}$. The dijet mass resolution is approximately 10% for dijet masses above 150 GeV/c². Our data sample was obtained using four triggers that required at least one jet with

uncorrected cluster transverse energies of 20, 50, 70 and 100 GeV, respectively. After jet energy corrections these trigger samples were used to measure the dijet mass spectrum above 150, 217, 292 and 388 GeV/c², respectively. At these mass thresholds the corresponding trigger efficiencies were greater than 93%. The four data samples corresponded to integrated luminosities of 0.087, 2.2, 11 and 87 pb⁻¹ after prescaling. We selected events with two or more jets and required that the two leading jets have pseudorapidity $|\eta_1| < 2$ and $|\eta_2| < 2$ and a scattering angle in the dijet center-of-mass frame $|\cos\theta^*| = |\tanh[(\eta_1 - \eta_2)/2]| < 2/3$. The $\cos\theta^*$ requirement ensures uniform acceptance as a function of mass and reduces the QCD background which peaks at $|\cos\theta^*| = 1$. To maintain the projective nature of the calorimeter towers, the z position of the event vertex was required to be within 60 cm of the center of the detector; this cut removed 7% of the events. Backgrounds from cosmic rays, beam halo, and detector noise were removed by requiring $\cancel{E}_T/\sqrt{\sum E_T} < 6$ GeV^{1/2} and $\sum E < 2$ TeV, where \cancel{E}_T is the missing transverse energy, $\sum E_T$ is the total transverse energy, and $\sum E$ is the total energy in the event.

To identify jets originating with a b -quark we require that tracks reconstructed in the CTC and SVX form a secondary–vertex, displaced from the event vertex. In the secondary–vertex algorithm, described elsewhere [7], we tightened the transverse momentum (p_T) requirements on the tracks as a function of dijet mass to reduce backgrounds at high mass [8]. The highest p_T track in a reconstructed vertex was required to have a p_T of at least 2 GeV/c for dijets with a mass less than 321 GeV/c². This cut was tightened incrementally as a function of dijet mass to 5 GeV/c for dijets

with a mass greater than $470 \text{ GeV}/c^2$. For secondary-vertices formed from only two tracks, we additionally required that the tracks have a minimum p_T of at least $1 \text{ GeV}/c$ for dijets with mass less than $321 \text{ GeV}/c^2$, rising to $2 \text{ GeV}/c$ for dijets with mass greater than $388 \text{ GeV}/c^2$. We required both jets in the dijet to have a displaced secondary-vertex (a b -tag). The efficiency of our b -tagging algorithm was determined from a Monte Carlo simulation of detector response to the decay of a heavy object to $b\bar{b}$. The simulation was tuned to reproduce the observed tracking efficiency [8]. The efficiency for b -tagging a heavy object decaying to $b\bar{b}$ decreases from 11% to 2.5% as the dijet mass increases from 200 to $650 \text{ GeV}/c^2$. The efficiency decreases as the dijet mass increases because the secondary-vertex resolution and acceptance degrade as the distance from the event vertex increases and because the tracking efficiency degrades as the density of tracks within a jet increases.

In Fig. 1 we present the inclusive dijet mass distribution for untagged and double- b -tagged dijets with $|\eta| < 2$ and $|\cos \theta^*| < 2/3$. The mass distributions have been corrected for the trigger, z -vertex, and b -tagging inefficiencies previously discussed. We plot the differential cross section versus the mean dijet mass, m , in bins of width approximately equal to the mass resolution (RMS $\sim 10\%$). The b -tagged data are compared to a smooth parameterization and to a QCD prediction. The QCD prediction is for direct $b\bar{b}$ production from the PYTHIA Monte Carlo [9], with the b quarks decayed by the CLEO Monte Carlo QQ, and includes a simulation of the CDF detector. Direct $b\bar{b}$ production includes the processes $q\bar{q} \rightarrow b\bar{b}$ and $gg \rightarrow b\bar{b}$; other $b\bar{b}$ production processes do not contribute significantly. The QCD simulation

used CTEQ2L parton distributions [10] and a renormalization scale $\mu = P_T$.

To search for resonances, we fit the data to the shape of the $b\bar{b}$ Monte Carlo calculation and a new particle resonance. The $b\bar{b}$ prediction multiplied by a factor of 1.7 fits the data well ($\chi^2/\text{DF} = 0.61$), as shown in Fig. 2 which also shows the predicted line shape for narrow resonances and topgluons. Narrow resonances were modeled with a PYTHIA simulation of a Z' decaying to $b\bar{b}$ followed by the CDF detector simulation. The mass resolution is dominated by a Gaussian distribution from jet energy resolution and a long tail towards low mass from QCD radiation. Since the natural width of the Z' is significantly smaller than the reconstructed width, these mass resonance curves were used to model the shape of all narrow resonances decaying to $b\bar{b}$. Topgluons were modeled using a PYTHIA simulation, in which we inserted the parton-level sub-process cross section for topgluons [2], followed by the CDF detector simulation. We simulated topgluons with width $\Gamma = 0.3M$, $0.5M$, and $0.7M$. There is no evidence in the data for either narrow or wide resonances decaying to $b\bar{b}$.

Systematic uncertainties on the cross section for observing a new particle in the CDF detector are shown in Fig. 3. Each systematic uncertainty on the fitted signal cross section was determined by varying the source of uncertainty by $\pm 1\sigma$ and refitting. The sources of uncertainty presented in Fig. 3 are the jet energy scale uncertainty, the b -tagging efficiency, the effect of QCD radiation on the mass resonance line shape, the shape of the $b\bar{b}$ background predicted by QCD, and other sources including trigger efficiency, jet energy resolution for narrow resonances, relative jet

energy corrections between different parts of the CDF calorimeter, and luminosity. The dominant systematic uncertainty at low mass is a 3% uncertainty in the jet energy scale. The dominant systematic uncertainty at high mass was the uncertainty in the b -tagging efficiency, which varied from 14% at low mass to 24% at high mass. The uncertainty on the shape of the $b\bar{b}$ background, from using various parton distributions, produced a relatively small uncertainty in the cross section limits compared to the dominant sources discussed above, which primarily affect the signal. Other possible sources of background, such as mistags or charm, may contribute to the normalization but are expected to have a similar shape to $b\bar{b}$, and do not contribute significantly to the systematic uncertainty. The total systematic uncertainty was found by adding the individual sources in quadrature.

In the absence of evidence for new physics we proceeded to set upper limits on the cross section for new particles. For each value of new particle mass in 50 GeV/c^2 steps from 200 to 750 GeV/c^2 , we performed a binned maximum likelihood fit of the data to the background shape and the mass resonance shape. We convoluted each of the Poisson likelihood distributions with the corresponding total Gaussian systematic uncertainty, and found the 95% confidence level (CL) upper limit presented in Table I.

In Fig. 4 we plot our measured upper limit on the cross section times branching ratio as a function of new particle mass in 50 GeV/c^2 steps. The limit is compared to lowest-order theoretical predictions for the cross section times branching ratio for new particles decaying to $b\bar{b}$. New-particle decay angular distributions are included in the

calculations, and we required $|\eta| < 2$ and $|\cos \theta^*| < 2/3$ for all predictions. For narrow resonances we exclude the color octet technirho in the mass interval $350 < M < 440$ GeV/c^2 . In addition, our limits for narrow resonances are applicable to any particle decaying to $b\bar{b}$ with a width significantly less than our detector resolution of 10%. Constructive interference between topgluons and normal gluons causes the signal cross section to rise at low $b\bar{b}$ mass, m , and results in a total cross section integrated over all m that is not well defined. To avoid this, the total cross section for a topgluon of mass M is defined as the cross section in the region $0.5M < m < 1.5M$, for both the experimental upper limit and the theoretical prediction. We exclude topgluons of width $\Gamma = 0.3M$ in the mass range $280 < M < 670$ GeV/c^2 , of width $\Gamma = 0.5M$ in the mass range $340 < M < 640$ GeV/c^2 , and of width $\Gamma = 0.7M$ in the mass range $375 < M < 560$ GeV/c^2 .

In conclusion, the measured $b\bar{b}$ mass spectrum does not contain evidence for a mass peak from a new particle resonance. We have presented model independent limits on the cross section for a narrow resonance, and set specific mass limits on narrow color-octet technirhos and topgluons of various widths.

We thank the Fermilab staff and the technical staffs of the participating institutions for their vital contributions. This work was supported by the U.S. Department of Energy and National Science Foundation; the Italian Istituto Nazionale di Fisica Nucleare; the Ministry of Education, Science and Culture of Japan; the Natural Sciences and Engineering Research Council of Canada; the National Science Council of the Republic of China; and the A. P. Sloan Foundation.

References

- [1] C. T. Hill, Phys. Lett. B **345**, 483 (1995) and C. T. Hill and S. J. Parke, Phys. Rev. D **49**, 4454 (1994).
- [2] E. Eichten and K. Lane, New Directions for High-Energy Physics, edited by G. Cassel, L. Gennari, and R. Siemann, 1997, page 1006-1009.
- [3] F. Abe *et al.*, Phys. Rev. Lett. **74**, 2900 (1995) and Phys. Rev. D **51**, R949 (1995), and references therein.
- [4] R. Shanidze, E. Chikovani, V. Kartvelishvili and G. Shaw, Phys. Rev. D **53**, 6653 (1994).
- [5] F. Abe *et al.*, Nucl. Instrum. and Methods **A271**, 387 (1988); F. Abe *et al.*, Phys. Rev. D **50**, 2966 (1994).
- [6] F. Abe *et al.*, Phys. Rev. D **45**, 1448 (1992).
- [7] F. Abe *et al.*, Phys. Rev. Lett. **74**, 2626 (1995).
- [8] K. D. Hoffman, Ph.D. thesis, Purdue University, 1998.
- [9] T. Sjöstrand, Comput. Phys. Commun. **82**, 74 (1994).
- [10] J. Botts *et al.*, Phys. Lett. **B304**, 159 (1993).

Mass (GeV/c ²)	Narrow				Topgluons			
	$\Gamma/M < 0.1$		$\Gamma/M = 0.3$		$\Gamma/M = 0.5$		$\Gamma/M = 0.7$	
	σ limit (pb)							
200	8.7×10^2	1.7×10^3	2.4×10^3	3.7×10^3				
250	1.6×10^2	3.8×10^2	6.0×10^2	9.6×10^2				
300	3.5×10^1	8.1×10^1	1.4×10^2	2.1×10^2				
350	1.2×10^1	2.8×10^1	4.0×10^1	5.1×10^1				
400	4.8	1.3×10^1	1.7×10^1	1.9×10^1				
450	3.2	7.6	9.9	1.2×10^1				
500	3.1	5.5	6.6	8.0				
550	3.3	4.5	4.9	5.8				
600	3.3	4.0	3.9	4.3				
650	3.3	3.5	3.4	3.4				
700	3.5	3.2	3.0	2.9				
750	4.0	3.0	2.9	2.8				

Table 1: The 95% CL upper limit on the cross section times branching ratio for new particles decaying to $b\bar{b}$ as a function of new particle mass for narrow resonances and for topgluons of three different widths (see text).

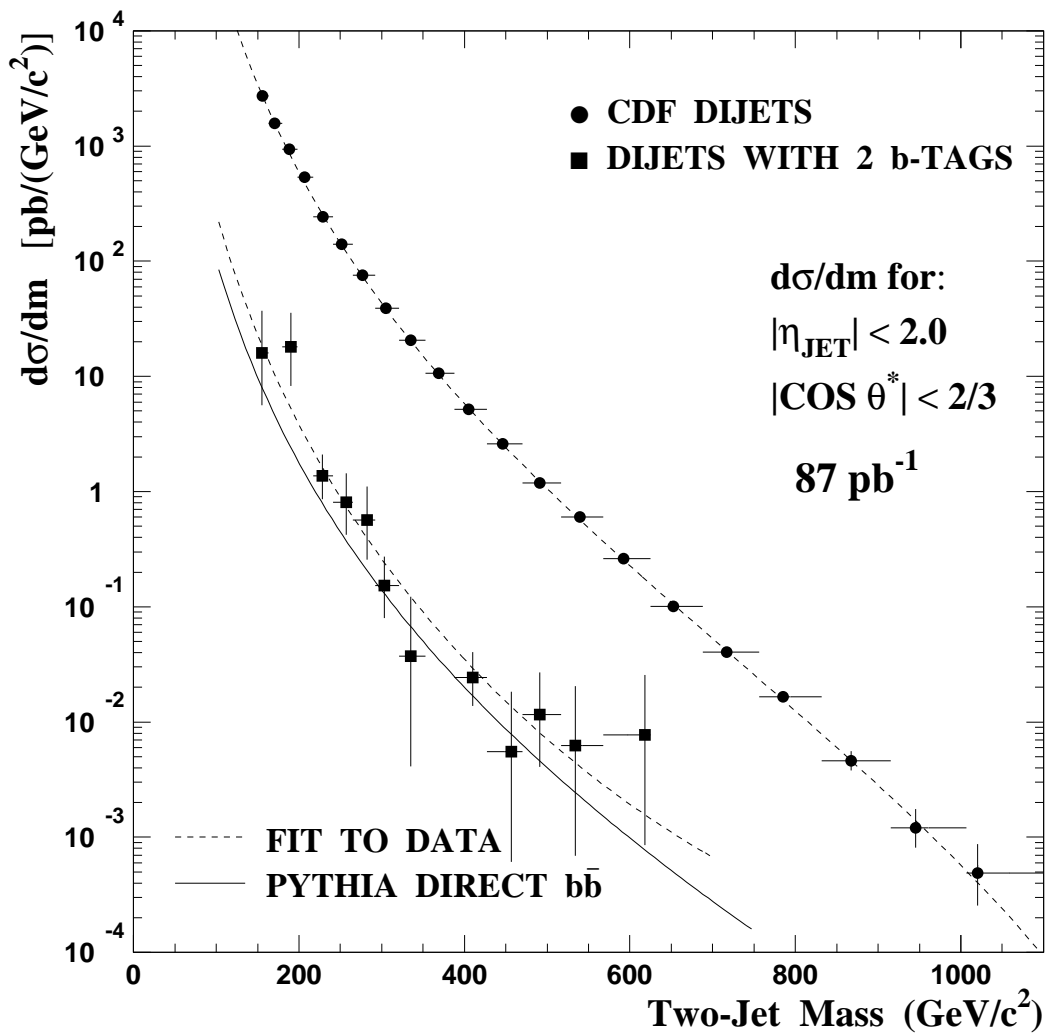


Figure 1: The dijet mass distribution (circles) and double- b -tagged dijet mass spectrum (boxes) compared to a fit to a smooth parameterization (dashed curves). Also shown is a QCD prediction for $b\bar{b}$ production (solid curve).

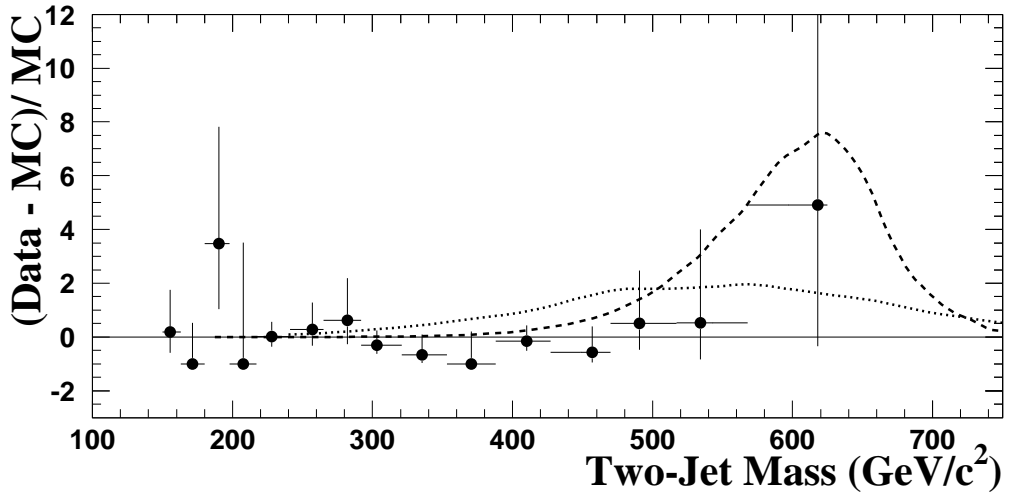


Figure 2: The fractional difference between the double- b -tagged dijet mass distribution (points) and a background prediction (solid line) is compared to a simulation of a $600 \text{ GeV}/c^2$ narrow resonance (dashed curve) and a $600 \text{ GeV}/c^2$ topgluon of width $\Gamma = 0.5M$ (dotted curve) in the CDF detector. The background has been normalized to fit the data and the resonances have each been normalized to the 95% CL upper limit on the cross section for a $600 \text{ GeV}/c^2$ resonance.

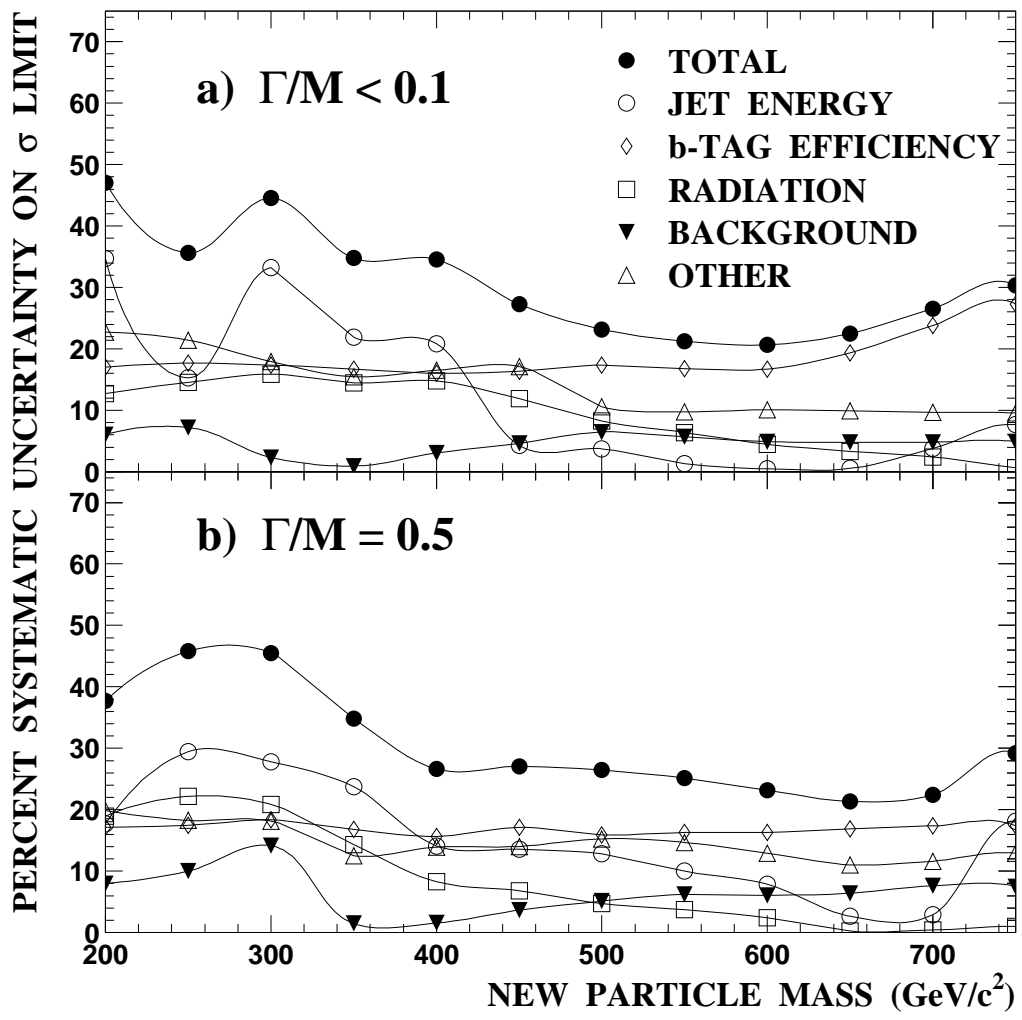


Figure 3: Systematic uncertainties on the cross section upper limit for a) narrow resonances and b) topgluons of width $\Gamma = 0.5M$ as a function of mass.

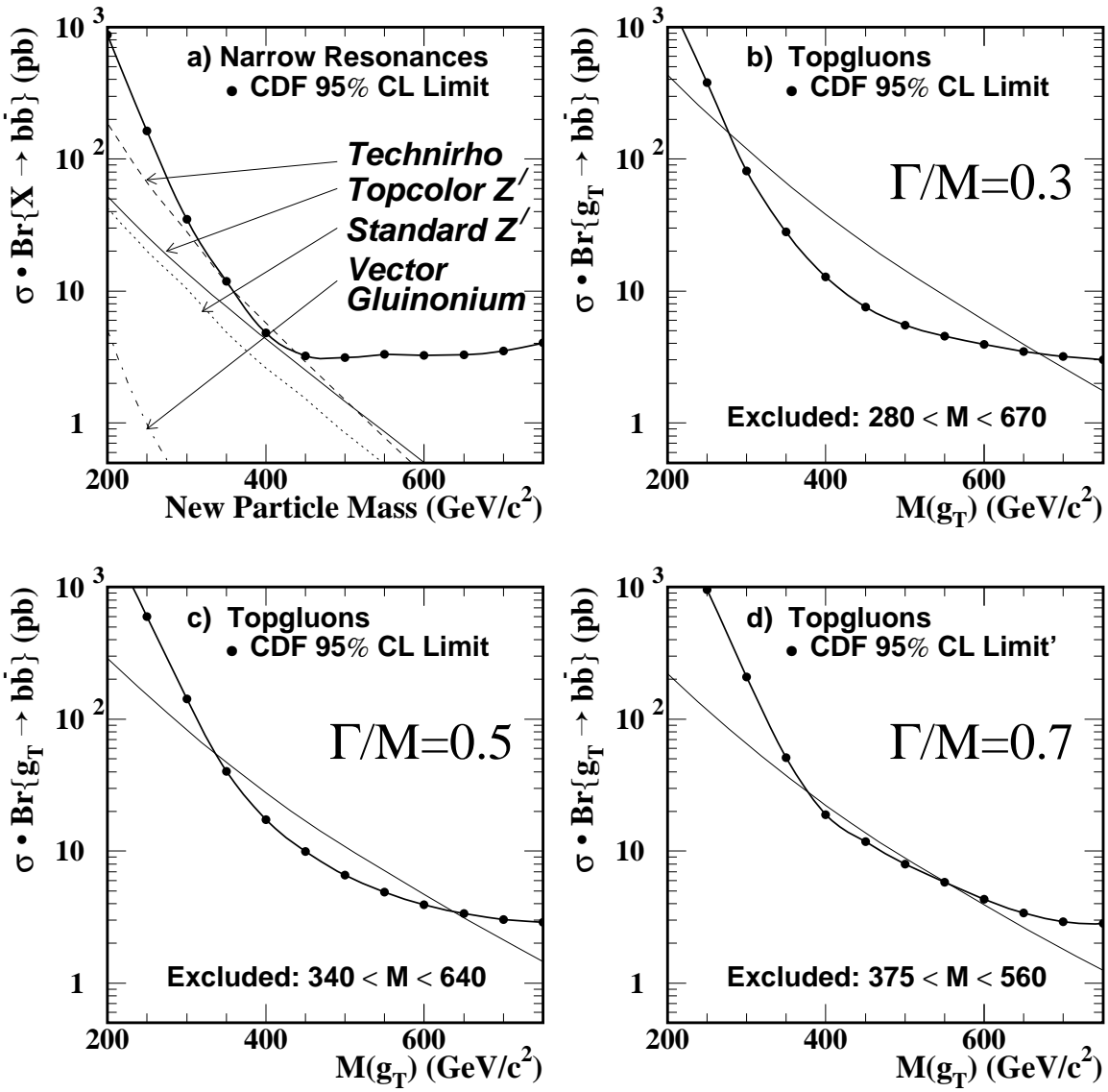


Figure 4: The 95% CL upper limit on the cross section times branching ratio (points) for a) narrow resonances, and topgluons of width b) $\Gamma = 0.3M$, c) $\Gamma = 0.5M$, and d) $\Gamma = 0.7M$ is compared to theoretical predictions (curves).